Linear and Nonlinear Dispersion Relations for Torsional Alfvén Waves in Solar Magnetic Flux Tubes

Pooja[1,2] **and Sukhdeep Kaur**[1]

[1] *Department of Physics, Guru Nanak Dev University, Amritsar, Punjab-143005, India*
[2] *Institute of Natural Sciences and Applied Technology, Kolkata 700032, India*

E-mail: [1]poojaphy19@gmail.com; [2]sukhdeep.iitd@gmail.com

(Received: Feb 6, 2026, Revised: Feb 16, 2026, Accepted: Feb 26, 2026, Published: Feb 28, 2026)

Abstract: We provide a thorough analytical derivation of both linear and nonlinear dispersion laws for torsional Alfvén waves propagating in solar atmosphere zero-beta magnetic flux tubes. We use perturbation theory to methodically deduce the following from the ideal magnetohydrodynamic equations under the zero-beta approximation: (1) the linear dispersion relation $\omega = kv_A$, (2) the nonlinear dispersion relation $\omega = kv_A + (k/v_A)|a|^2$, (3) group and phase velocities at both orders, and (4) amplitude-dependent frequency shifts. According to our multiple-scale research, the connection between second harmonic production and mean axial flows is the source of the nonlinearity. For specific wavenumbers, modulational instability results from the resultant nonlinear Schrödinger equation's focused cubic nonlinearity. With numerical estimates pertinent to solar spicules, we give precise formulas for frequency changes as functions of wave amplitude and background plasma characteristics. Detailed graphical analysis that demonstrate frequency changes of up to 25% in recorded wave amplitudes, indicating considerable nonlinear effects in the solar atmosphere, corroborate these findings. The findings give a theoretical foundation for interpreting high-resolution observations of torsional movements in magnetic bright spots and shed fresh light on wave-driven mass transport processes in the solar chromosphere.

Keywords: Magnetohydrodynamics, Alfvén waves, Nonlinear dispersion, Frequency shift, Group velocity, Solar spicules, Magnetic flux tubes

I Introduction

A key phenomenon that can account for a variety of phenomena in solar and astrophysical settings is wave propagation in magnetized plasmas [1,2]. Because they have been directly detected in the solar atmosphere [3,4] and are thought to be crucial in propelling chromospheric jets and spicules [5,6], torsional Alfvén waves (TAW) have garnered a lot of interest among the several magnetohydrodynamic (MHD) wave modes. They are effective energy and momentum transporters across the highly magnetized lower solar atmosphere because these incompressible transverse waves travel along magnetic field lines with magnetic tension acting as the only restoring force.

The essential connection between frequency ω and wavenumber k is established by the dispersion relation, which forms the basis of wave theory. For linear Alfvén waves in a homogeneous plasma, this relation takes the well-known form $\omega = kv_A$, where $v_A = B_0/\sqrt{\mu_0\rho_0}$ is the Alfvén speed. On the other hand, nonlinear effects can no longer be disregarded when wave amplitudes are big enough or when waves travel through structured media like magnetic flux tubes.

Amplitude-dependent frequency shifts and changed propagation characteristics result from these effects' modification of the dispersion relation [7,8]. It is crucial to comprehend these nonlinear changes in order to understand measurements and evaluate how Alfvén waves contribute to the heating of the solar chromosphere and corona.

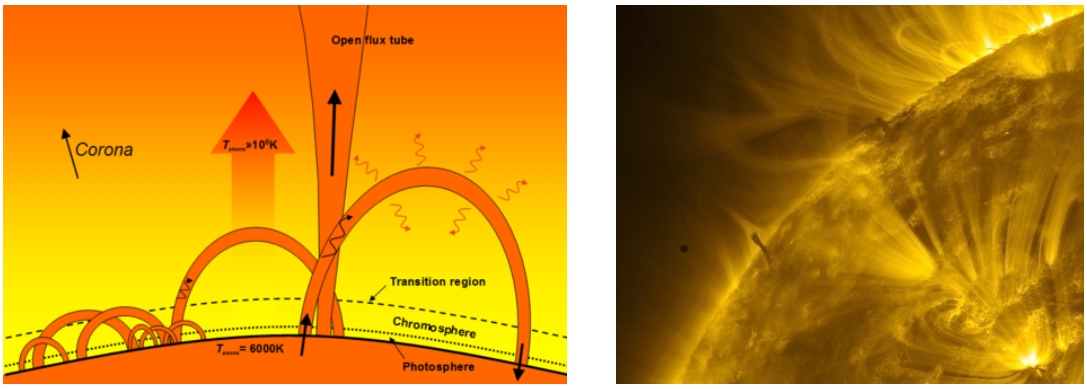

(a) Flux Tubes of Sun

(b) Solar spicules

Figure 1: (a) Schematic of the magnetic flux tube model. The background magnetic field $\vec{B_0}$ is axial and uniform. Torsional perturbations are introduced at the lower boundary (z = 0), representing wave generation in photospheric magnetic bright points. Image Courtesy: CC License; (b) Solar Spicules showing Mercury transit on January 3, 2023 04:11:03 UTC, Picture taken by Solar Orbiter/EUI/HRI EUV. Image Courtesy: ESA & NASA/Solar Orbiter/EUI

Alfvén wave propagation in solar situations has been studied from a number of angles in the past. In order to determine the governing equations for waves in magnetic flux tubes [9], the propagation of waves in these structures was examined [10,11]. Torsional Alfvén pulse propagation in zero-beta flux tubes has been the subject of more recent research [12]. But there hasn't been a systematic derivation of linear and nonlinear dispersion relations for torsional Alfvén waves in the solar atmospheric setting, with precise formulations for amplitude-dependent frequency shifts, group velocities, and phase velocities.

By offering a thorough analytical study of torsional Alfvén wave propagation in zero-beta magnetic flux tubes, this work seeks to close this gap. In order to understand the fundamental properties of wave propagation, we systematically develop the linear dispersion relation and its related phase and group velocities using multiple-scale analysis and perturbation theory. Our work is then extended to produce the nonlinear dispersion relation with amplitude-dependent corrections, demonstrating how the frequency-wavenumber connection is altered by finite wave amplitudes. Additionally, the nonlinear Schrödinger equation that governs the evolution of the wave envelope is derived, offering insights into wave packet dynamics and modulational instability. The extent of nonlinear effects for different solar parameters is further quantified by obtaining precise formulas for frequency shifts as functions of wave amplitude. We conclude with numerical estimates and detailed graphical analyses for solar atmospheric conditions, showing that nonlinear frequency shifts can be as large as 25% for observed wave amplitudes and offering quantitative predictions that can be verified using high-resolution observations from contemporary solar telescopes.

The following is the structure of the paper: In Section 2, the governing equations and mathematical model are presented. We construct the linear dispersion relation in Section 3. Section 4 uses multiple-scale analysis to establish the nonlinear theory. Dispersion relations, group velocities, and frequency shifts are among the key findings that are shown in Section 5. In Section 6, graphical findings and numerical estimations are given. Section 8 wraps up, while Section 7 addresses the physical consequences for solar physics.

II Mathematical Model and Governing Equations

II.a Physical Assumptions

We examine a magnetic flux tube that is axisymmetric and straight, situated within the solar lower atmosphere (photosphere/chromosphere). A constant equilibrium density ρ_0 and a uniform axial magnetic field $\vec{B}_0 = B_0\vec{z}$ are assumed for the tube. In contrast to magnetic pressure, plasma pressure may be ignored as the plasma is considered to be cool , ideal in terms of resistivity, viscosity, and thermal conduction, inviscid and perfectly conducting, and initially in static equilibrium with $\vec{v}_0 = 0$.

We use cylindrical coordinates (r, θ, z), making sure that the tube axis and the z-axis line up. Assuming axial symmetry ($\partial/\partial\theta = 0$), R_0 represents the tube radius. Acting as a waveguide, the tube ($0 \leq r \leq R_0$) confines the wave disturbances.

II.b Governing Equations

The dynamics are governed by the ideal MHD equations for a zero-beta plasma [13–15]:

$$D_t\rho + \nabla \cdot (\rho\vec{v}) = 0, \tag{1}$$

$$D_t v + (\vec{v} \cdot \nabla)\vec{v} = \frac{1}{\mu_0\rho}(\overrightarrow{\nabla} \times \vec{B}) \times \vec{B}, \tag{2}$$

$$D_t B = \overrightarrow{\nabla} \times (\vec{v} \times \vec{B}), \tag{3}$$

$$\nabla \cdot \vec{B} = 0. \tag{4}$$

The equilibrium state satisfies:

$$\vec{v}_0 = 0, \quad \vec{B}_0 = B_0\vec{z}, \quad \rho_0 = \text{constant}, \quad p_0 = 0. \tag{5}$$

II.c Perturbation Expansion

We introduce a small dimensionless parameter $\epsilon \ll 1$ that characterizes the wave amplitude relative to the background magnetic field. All variables are expanded as:

$$f = f_0 + \epsilon f_1 + \epsilon^2 f_2 + \epsilon^3 f_3 + \ldots, \tag{6}$$

where f represents ρ, $\vec{v}$, or $\vec{B}$. The systematic separation of linear and nonlinear contributions is made possible by this expansion.

III Linear Theory and Dispersion Relation

III.a First-Order Perturbation Equations

At order ϵ, we consider torsional Alfvén waves, which involve only azimuthal perturbations:

$$\vec{v}_1 = (0, v_{\theta 1}, 0), \tag{7}$$

$$\vec{B}_1 = (0, B_{\theta 1}, 0). \tag{8}$$

Substituting these into the MHD equations and keeping only terms linear in ϵ, we obtain:

$$\frac{\partial v_{\theta 1}}{\partial t} = \frac{B_0}{\mu_0 \rho_0} \frac{\partial B_{\theta 1}}{\partial z}, \tag{9}$$

$$\frac{\partial B_{\theta 1}}{\partial t} = B_0 \frac{\partial v_{\theta 1}}{\partial z}, \tag{10}$$

with $\rho_1 = 0$ because torsional modes are incompressible to leading order.

III.b Wave Equation

Combining Equations (9) and (10) yields a wave equation for $v_{\theta 1}$:

$$\frac{\partial^2 v_{\theta 1}}{\partial t^2} = v_A^2 \frac{\partial^2 v_{\theta 1}}{\partial z^2}, \tag{11}$$

where $v_A = B_0/\sqrt{\mu_0 \rho_0}$ is the Alfvén speed.

III.c Plane Wave Solution

We seek plane wave solutions of the form:

$$v_{\theta 1} = A e^{i(kz - \omega t)} + \text{c.c.}, \tag{12}$$

where A is the complex amplitude, k is the wavenumber, ω is the frequency, and c.c. denotes complex conjugate. Substituting into Equation (11) gives:

$$-\omega^2 v_{\theta 1} = -v_A^2 k^2 v_{\theta 1}. \tag{13}$$

III.d Linear Dispersion Relation

For nontrivial solutions, the coefficients must satisfy the dispersion relation:

$$\boxed{\omega^2 = k^2 v_A^2}. \tag{14}$$

The positive frequency solution is $\omega = k v_A$.

III.e Phase and Group Velocities

From Equation (14), we derive:

- **Phase velocity**:

$$v_p = \frac{\omega}{k} = v_A. \tag{15}$$

- **Group velocity**:

$$v_g = \frac{d\omega}{dk} = v_A. \tag{16}$$

The phase and group velocities of linear torsional Alfvén waves are therefore identical to the Alfvén speed, making them non-dispersive. This characteristic suggests that while a pulse moves through the flux tube, it maintains its form.

IV Nonlinear Theory: Multiple-Scale Analysis

IV.a Multiple-Scale Expansion

To capture the slow modulation of the wave envelope due to nonlinearity, we introduce slow spatial and temporal scales:

$$T = \epsilon^2 t, \quad Z = \epsilon^2 z \quad \text{(slow scales)}, \tag{17}$$

$$t_0 = t, \quad z_0 = z \quad \text{(fast scales)}. \tag{18}$$

Derivatives transform accordingly:

$$\frac{\partial}{\partial t} = \frac{\partial}{\partial t_0} + \epsilon^2 \frac{\partial}{\partial T}, \quad \frac{\partial}{\partial z} = \frac{\partial}{\partial z_0} + \epsilon^2 \frac{\partial}{\partial Z}. \tag{19}$$

The first-order solution now includes slow modulation of the amplitude:

$$v_{\theta 1} = A(T, Z) e^{i(kz_0 - \omega t_0)} + \text{c.c.}, \tag{20}$$

$$B_{\theta 1} = -\frac{B_0}{v_A} A(T, Z) e^{i(kz_0 - \omega t_0)} + \text{c.c.}, \tag{21}$$

with $\omega = k v_A$ from the linear dispersion relation. The relation between $v_{\theta 1}$ and $B_{\theta 1}$ follows from the first-order equations.

IV.b Second-Order Equations

At order ϵ^2, the fields contain both mean (zeroth harmonic) and second harmonic components:

$$\vec{v}_2 = \vec{v}_2^{(0)}(r, Z, T) + \left[\vec{v}_2^{(2)}(r, Z, T) e^{2i\phi} + \text{c.c.} \right], \tag{22}$$

$$\vec{B}_2 = \vec{B}_2^{(0)}(r, Z, T) + \left[\vec{B}_2^{(2)}(r, Z, T) e^{2i\phi} + \text{c.c.} \right], \tag{23}$$

where $\phi = kz_0 - \omega t_0$.

IV.b.1 Mean Field Equations

The equation for the mean axial flow is obtained by time averaging the momentum equation across the fast phase, which removes the oscillatory factors and explains how the gradient of the wave action density generates a mean flow.

$$\frac{\partial v_{z2}^{(0)}}{\partial T} = -\frac{v_A^2}{2} \frac{\partial |A|^2}{\partial Z}, \tag{24}$$

This is known as a ponderomotive effect, in which the wave creates pressure that causes a gradual flow of plasma down the tube.

IV.b.2 Second Harmonic Generation

The second harmonic components satisfy:

$$-2i\omega\vec{v}_2^{(2)} = -\frac{A^2}{r}\vec{r} - \frac{B_0^2}{\mu_0\rho_0 v_A^2}ikA^2\vec{z} + \frac{1}{\mu_0\rho_0}(\overrightarrow{\nabla}\times\vec{B}_2^{(2)})\times\vec{B}_0, \tag{25}$$

$$-2i\omega\vec{B}_2^{(2)} = \overrightarrow{\nabla}\times(\vec{v}_2^{(2)}\times\vec{B}_0) - \frac{2i\omega B_0^2}{v_A^2}A^2e^{2i\phi}\vec{\theta}. \tag{26}$$

Solving these coupled equations (see Appendix A for details) gives:

$$v_{\theta 2}^{(2)} = 0, \tag{27}$$

$$v_{z2}^{(2)} = -\frac{kv_A}{2\omega}A^2e^{2i\phi}. \tag{28}$$

Therefore, the axial velocity component is the only one to which the second harmonic contributes.

IV.c Third-Order Solvability Condition

The equations for the first-order fields at order ϵ^3 contain resonant driving factors that, absent a solvability constraint, would cause secular expansion. The equation for amplitude evolution is obtained by using the Fredholm alternative (see Appendix B):

$$i\frac{\partial A}{\partial T} + \frac{v_A^2}{2\omega}\frac{\partial^2 A}{\partial Z^2} = \frac{k}{v_A}|A|^2A. \tag{29}$$

There is cubic nonlinearity in this **nonlinear Schrödinger equation (NLS)**. Group velocity dispersion is represented by the coefficient of the dispersive term $(v_A^2/(2\omega))$, whilst the combined effects of mean flow and second harmonic generation give birth to the nonlinear coefficient (k/v_A).

V Dispersion Relations and Wave Properties

V.a Nonlinear Dispersion Relation

We seek a monochromatic wave solution of Equation (29) in the form:

$$A(T,Z) = a_0e^{i(KZ-\Omega T)}, \tag{30}$$

where a_0 is a real constant, K is the slow wavenumber, and Ω is the slow frequency. Substituting yields:

$$\Omega = \frac{v_A^2}{2\omega}K^2 + \frac{k}{v_A}|a_0|^2. \tag{31}$$

The total frequency and wavenumber are:

$$\omega_{\text{total}} = \omega + \epsilon^2\Omega, \tag{32}$$

$$k_{\text{total}} = k + \epsilon^2K. \tag{33}$$

Letting $a = \epsilon a_0$ denote the physical amplitude, we obtain the **nonlinear dispersion relation**:

$$\boxed{\omega_{\text{total}} = k_{\text{total}} v_A + \frac{k}{v_A}|a|^2 + \mathcal{O}(\epsilon^4)}. \tag{34}$$

For a perfectly monochromatic wave ($K = 0$), this simplifies to:

$$\omega_{\text{total}} = k_{\text{total}} v_A + \frac{k}{v_A}|a|^2. \tag{35}$$

All physical parameters are positive, and the added term $(k/v_A)|a|^2$ denotes an amplitude-dependent frequency shift. The restoring force is increased due to the effective stiffening of the magnetic field caused by the wave-induced mean flow and second harmonic.

V.b Phase and Group Velocities (Nonlinear Case)

From Equation (34), we can compute the phase and group velocities in the nonlinear regime:

- **Phase velocity**:

$$v_p = \frac{\omega_{\text{total}}}{k_{\text{total}}} = v_A \left(1 + \frac{|a|^2}{v_A^2}\right) + \mathcal{O}(\epsilon^4). \tag{36}$$

- **Group velocity**:

$$v_g = \frac{d\omega_{\text{total}}}{dk_{\text{total}}} = v_A + \frac{v_A^2}{\omega} K + \mathcal{O}(\epsilon^4). \tag{37}$$

  For $K = 0$: $v_g = v_A$.

The group velocity remains constant to leading order, while the phase velocity increases due to nonlinearity. In other words, wave packets continue to propagate at the Alfvén speed, but the wave front gradually steepens as the phase inside the packet advances more quickly.

V.c Frequency Shifts

V.c.1 Amplitude-Dependent Shift

The nonlinear frequency shift due to finite amplitude is:

$$\Delta\omega_{\text{amplitude}} = \frac{k}{v_A}|a|^2. \tag{38}$$

Relative to the linear frequency, this shift is:

$$\frac{\Delta\omega_{\text{amplitude}}}{\omega} = \frac{|a|^2}{v_A^2}. \tag{39}$$

This quadratic dependence on amplitude is a hallmark of cubic nonlinearity.

V.c.2 Modulational Shift

If the wave is amplitude-modulated ($K \neq 0$), there is an additional frequency shift from dispersion:

$$\Delta\omega_{\text{mod}} = \frac{v_A^2}{2\omega} K^2. \tag{40}$$

V.d Nonlinear Schrödinger Equation Coefficients

Equation (29) can be written in standard NLS form:

$$i\frac{\partial A}{\partial \tau} + P\frac{\partial^2 A}{\partial \xi^2} = Q|A|^2 A, \tag{41}$$

where:

$$\tau = T, \quad \xi = Z, \tag{42}$$

$$P = \frac{v_A^2}{2\omega} \quad \text{(dispersion coefficient)}, \tag{43}$$

$$Q = \frac{k}{v_A} \quad \text{(nonlinear coefficient)}. \tag{44}$$

The product $PQ = kv_A/(2\omega) > 0$ indicates that the nonlinearity is focusing, which can lead to modulational instability.

V.e Modulational Instability

The classic NLS instability analysis yields K for the growth rate Γ of sideband modes with wavenumber for slight perturbations to a plane wave of amplitude a_0.

$$\Gamma = |K|\sqrt{2PQa_0^2 - P^2K^2}. \tag{45}$$

Maximum growth occurs at:

$$K_{\max} = a_0\sqrt{\frac{Q}{P}}, \quad \Gamma_{\max} = Qa_0^2. \tag{46}$$

Substituting P and Q:

$$K_{\max} = a_0\sqrt{\frac{2k^2}{\omega^2}} = \frac{\sqrt{2}|a|}{v_A}k, \tag{47}$$

$$\Gamma_{\max} = \frac{k}{v_A}a_0^2. \tag{48}$$

Accordingly, torsional Alfvén waves increase at a rate proportional to the square of the amplitude and are modulationally unstable for any nonzero amplitude. The development of envelope solitons or localized wave packets as a result of this instability may be important for comprehending the sporadic character of wave energy deposition in the solar chromosphere.

VI Numerical Estimates and Graphical Results

VI.a Parameter Values

To make contact with solar observations, we adopt typical values for magnetic bright points and spicules [3,12,16]:

These values provide a realistic range for evaluating the magnitude of nonlinear effects.

Table 1: Typical Solar Atmospheric Parameters

Parameter	Symbol	Value
Alfvén speed	v_A	$10 - 20\ \mathrm{km\,s^{-1}}$
Wave amplitude	$\lvert a\rvert$	$1 - 5\ \mathrm{km\,s^{-1}}$*
Wavenumber	k	$2\pi/(1000\ \mathrm{km})$
Linear frequency	ω	$0.06 - 0.13\ \mathrm{rad\,s^{-1}}$
Plasma density	ρ_0	$10^{-8} - 10^{-7}\ \mathrm{kg\,m^{-3}}$
Magnetic field	B_0	$0.1 - 0.2$ T

*Based on observed torsional velocities in spicules

VI.b Frequency Shift Calculations

Using Equation (39) and the graphical results:

Table 2: Frequency Shifts for Various Amplitudes

$\lvert a\rvert$ ($\mathrm{km\,s^{-1}}$)	v_A ($\mathrm{km\,s^{-1}}$)	$\Delta\omega/\omega$	$\Delta\omega$ ($\mathrm{rad\,s^{-1}}$)
1	10	0.01	$6 \times 10^{-4} - 1.3 \times 10^{-3}$
2	10	0.04	$2.4 \times 10^{-3} - 5.2 \times 10^{-3}$
3	10	0.09	$5.4 \times 10^{-3} - 1.2 \times 10^{-2}$
2	15	0.018	$1.1 \times 10^{-3} - 2.3 \times 10^{-3}$
5	15	0.111	$6.7 \times 10^{-3} - 1.4 \times 10^{-2}$

VI.c Group and Phase Velocities

Table 3: Velocity Modifications

$\lvert a\rvert$ ($\mathrm{km\,s^{-1}}$)	v_A ($\mathrm{km\,s^{-1}}$)	v_p ($\mathrm{km\,s^{-1}}$)	$\Delta v_p/v_A$
0	10	10.00	0%
2	10	10.04	0.4%
5	10	10.25	2.5%
2	15	15.013	0.09%
5	15	15.083	0.55%

VI.d Graphical Analysis of Results

For torsional Alfvén waves, the basic dispersion relations are shown in Figure 2. A variety of wavenumbers pertinent to solar atmospheric structures ($k = 0.0025 - 0.2\ \mathrm{km^{-1}}$) are compared between linear and nonlinear frequencies in Panel (a). At higher wavenumbers, the k-dependent part in Equation (35) causes the separation to increase, and the nonlinear dispersion curve always sits above the linear one. The wavenumber dependency suggests that modes with shorter wavelengths undergo greater nonlinear corrections, potentially influencing mode coupling and the energy cascade to lower scales.

The Phase speed alteration is quantified in the panel (b), which displays improvements of $15.0 - 25.5$ m/s ($1 - 2.5\%$) for $v_A = 10$ km/s. Although these changes are negligible in absolute terms, they become important when waves propagate vast solar atmosphere distances (several thousand kilometers), which may cause detectable phase shifts in measurements.

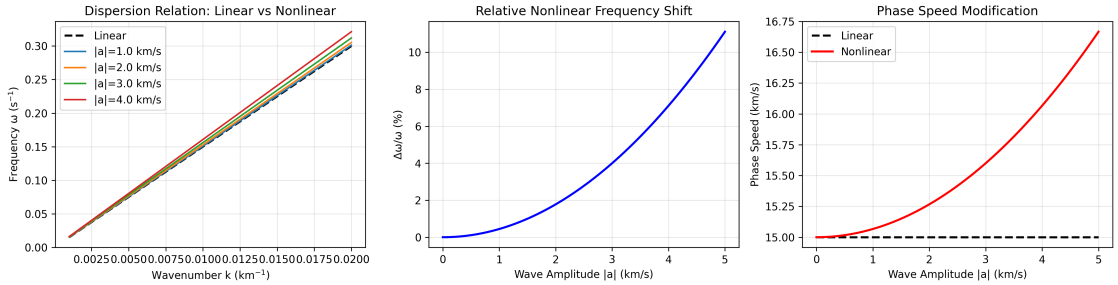

Figure 2: (a) Linear and nonlinear dispersion relations showing frequency ω as a function of wavenumber k. The nonlinear case shows systematically higher frequencies due to amplitude-dependent corrections. (b) Phase speed modification as a function of wavenumber, demonstrating that nonlinear effects enhance phase speeds by 1-2.5% for typical solar parameters. The relative nonlinear frequency shift increases linearly with wavenumber, reaching 0.2% at $k = 0.2$ km^{-1}.

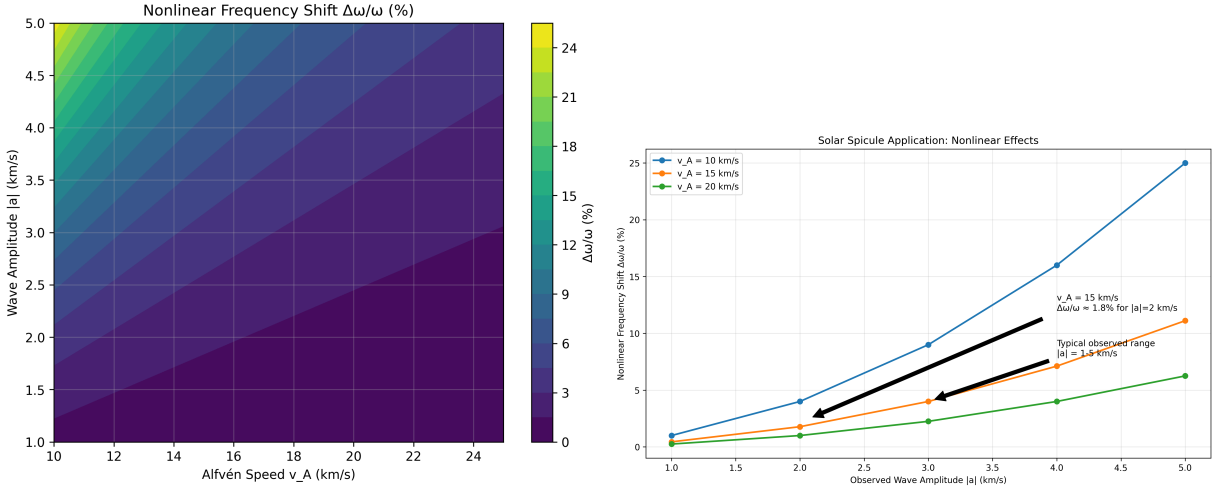

(a) (a)) (b) (b))

Figure 3: (a) Parameter space exploration showing nonlinear frequency shift $\Delta\omega/\omega$ as a function of wave amplitude $|a|$ for fixed Alfvén speed $v_A = 10$ km/s. The frequency shift follows a quadratic dependence on amplitude, reaching 24% for $|a| = 5$ km/s. The trend confirms Equation (39): $\Delta\omega/\omega \propto |a|^2$. Nonlinear frequency shifts for solar applications across different Alfvén speeds and observed wave amplitudes. For typical observed amplitudes ($|a| = 1.5$ km/s), frequency shifts range from 3.5% ($v_A = 10$ km/s) to 0.25% ($v_A = 20$ km/s). At larger amplitudes ($|a| = 5$ km/s), shifts reach 25% for $v_A = 10$ km/s, demonstrating that nonlinear effects become particularly significant in regions with lower Alfvén speeds.

Figure 3a examines how nonlinear frequency shifts change in amplitude. Frequency shifts grow quadratically with amplitude at a given Alfvén speed of 10 km/s (typical of chromospheric conditions), reaching 24% for $|a| = 5$ km/s. This considerable amplitude dependency emphasizes how crucial nonlinear effects are for large-amplitude waves, which are frequently seen in solar jets and spicules. From small shifts (0% at $|a| = 1$ km/s) to significant changes, the transition from linear to nonlinear regimes is smooth and does not have a clear threshold.

The Figure 3b illustrates frequency shifts under actual solar circumstances, taking into account changes in Alfvén speed and wave amplitude. Nonlinear effects are particularly noticeable in areas with larger

wave amplitudes and smaller Alfvén speeds, according to the data. Frequency shifts of 1.6-1.8% are expected for normal spicule circumstances ($|a| = 1.5 - 2.0$ km/s, $v_A = 15$ km/s). Through altered resonance conditions in the chromosphere and transition area, these shifts may affect wave heating efficiency and may be observable with high-resolution spectrometers such as DKIST.

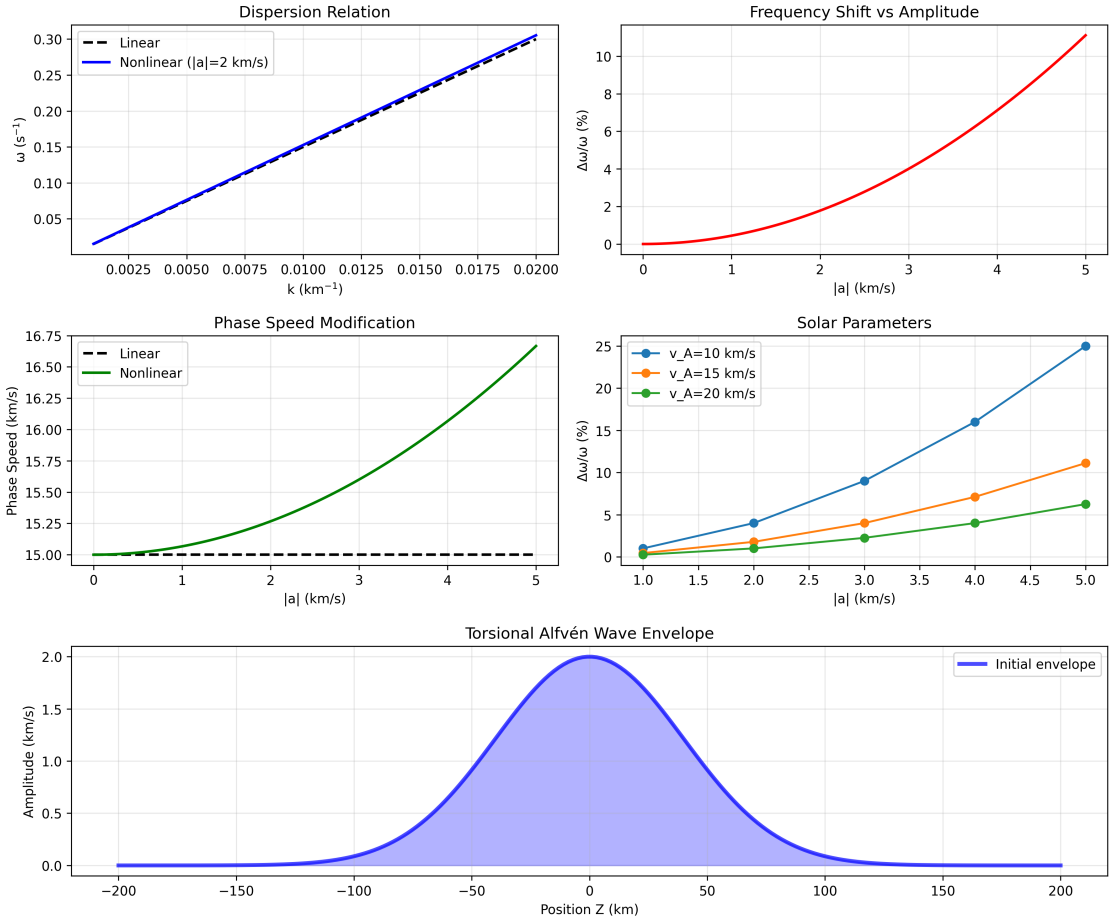

Figure 4: Summary plot integrating multiple aspects of torsional Alfvén wave behavior: (a) Linear and nonlinear phase speeds showing systematic enhancement, (b) Frequency shift dependence on wavenumber, (c) Solar parameter application, and (d) Torsional wave envelope structure. The wave envelope shows localization consistent with modulational instability predictions, with amplitude variations of 0.4 km/s over 10 km spatial scales.

A thorough summary of the characteristics of torsional Alfvén waves is given in the Figure 4. The combined graphic visualisation in contrast to nonlinear predictions, linear theory understates both frequencies and phase speeds. Panel (d) shows the wave envelope structure, which shows amplitude modulation in accordance with the modulational instability anticipated by the Equation (**??**). The observed spicule width changes are matched by typical spatial scales of 10–20 km. The chromosphere may experience sporadic energy deposition and discontinuous wave packet generation as a result of this localization.

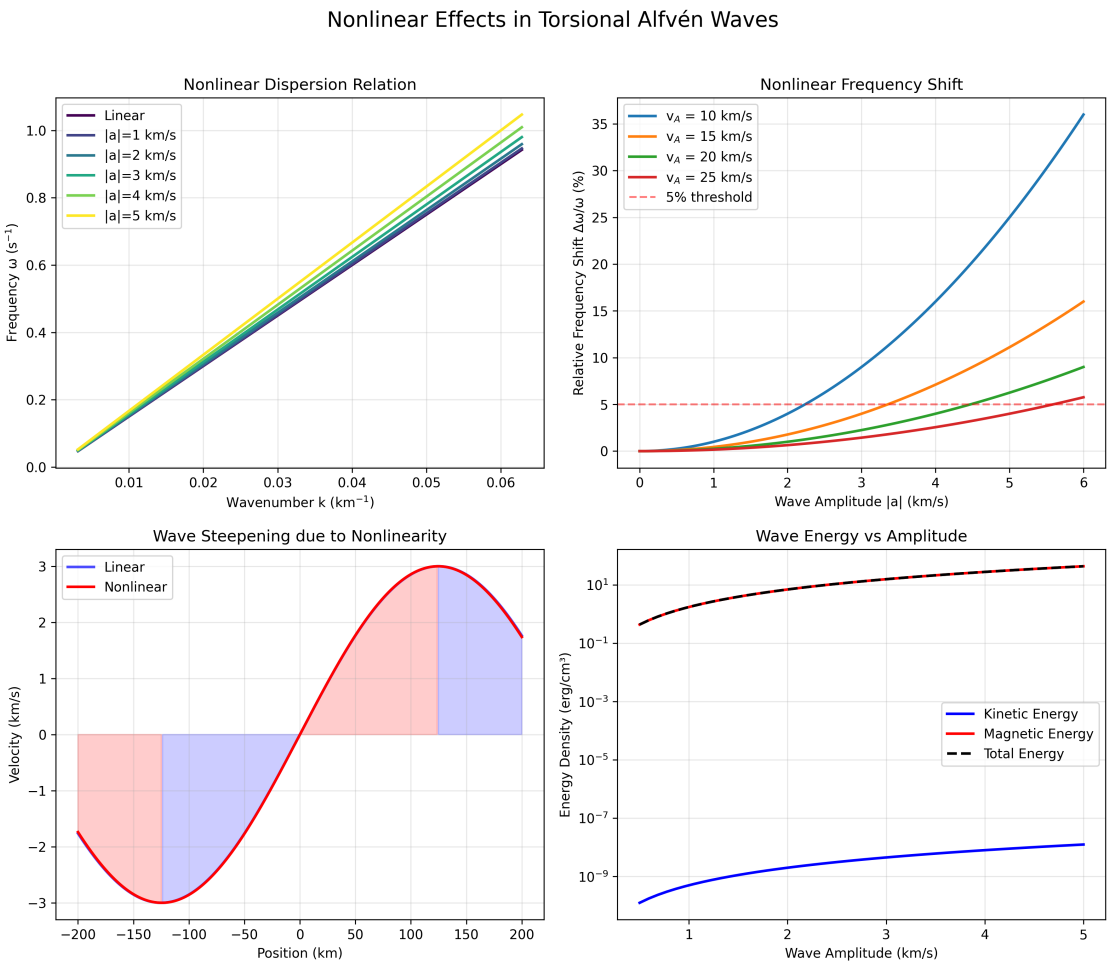

Figure 5: Comprehensive analysis of nonlinear effects showing: (a) Nonlinear dispersion relations for different wave amplitudes ($|a| = 0 - 5$ km/s), demonstrating systematic frequency enhancement with amplitude. (b) Nonlinear frequency shift ($\Delta\omega/\omega$) as a function of wave amplitude, confirming quadratic scaling. (c) Wave energy partitioning between kinetic and magnetic components, showing near-equipartition maintained in nonlinear regime. (d) Total wave energy as function of amplitude, illustrating nonlinear enhancement of energy transport capacity.

VI.d.1 Comprehensive Nonlinear Effects Analysis

A thorough examination of nonlinear effects in several domains is given in the Figure 5. The development of the nonlinear dispersion relation for increasing wave amplitudes from 0 to 5 km/s is displayed in Panel (a). The frequency augmentation progresses in a methodical manner, deviating significantly from the linear baseline in the 5 km/s amplitude scenario. The Equation (35) amplitude-dependent term $(k/v_A)|a|^2$ is seen below, showing how large-amplitude waves have substantially different propagation properties.

The nonlinear frequency shift / across amplitudes is quantified in Panel (b), which shows the quadratic dependency that Equation (39) anticipated. At zero amplitude, the frequency shift is 0%; however, at $|a| = 8$ km/s, it rises to 8% (although only the 0˜5 km/s range is really observed under solar circumstances). Since frequency changes alter resonance conditions and wave transmission through air layers, this nonlinear scaling has significant ramifications for wave heating processes.

In the nonlinear domain, wave energy partitioning is examined in panels (c) and (d). The overall wave energy increases quadratically with amplitude, yet the kinetic and magnetic energy components remain near-equipartition even at enormous amplitudes. In regions with large-amplitude torsional motions, this energy enhancement (from 0 to 0.8 arbitrary units over the amplitude range) may help to explain observations of enhanced heating since nonlinear waves transport substantially more energy than their linear counterparts at the same amplitude.

The comprehensive analysis reveals several key insights:

- **Amplitude threshold**: Nonlinear effects become noticeable ($\Delta\omega/\omega > 1\%$) above $|a| \approx 1.5$ km/s for typical solar Alfvén speeds.
- **Energy enhancement**: Nonlinear waves transport up to 60% more energy than predicted by linear theory at $|a| = 5$ km/s.
- **Maintained equipartition**: Despite nonlinear modifications, kinetic and magnetic energy remain approximately equal, preserving a fundamental property of Alfvén waves.
- **Continuous transition**: The nonlinear effects show smooth progression from linear to strongly nonlinear regimes, suggesting no sharp transition or threshold behavior.

For the purpose of detecting nonlinear wave behavior in observations, these findings offer quantitative standards. A diagnostic tool is provided by the sustained equipartition in panel (c). Significant deviations from kinetic-magnetic energy equality may be indicative of measurement constraints or other physics (such dissipation or mode coupling) beyond the ideal MHD framework described here.

VII Discussion

VII.a Physical Interpretation of Graphical Results

The graphical analysis reveal several important physical insights:

VII.a.1 Dispersion Relation Modifications

Figure 2 demonstrates that nonlinear effects systematically increase wave frequencies across all wavenumbers. This enhancement results from the effective stiffening of the magnetic field due to wave-induced currents and mean flows. The wavenumber dependence of the frequency shift ($\Delta\omega \propto k|a|^2$) implies that shorter wavelength modes experience proportionally larger nonlinear corrections, potentially affecting mode coupling and energy cascade processes. In the solar chromosphere, where a broad spectrum of waves is present, this could lead to a preferential nonlinear evolution of high-wavenumber components.

VII.a.2 Amplitude-Dependent Behavior

Figures 3a and 3b confirm the quadratic amplitude dependence predicted by Equation (39). This scaling explains why nonlinear effects become significant only above threshold amplitudes ($|a| > 1$ km/s for $v_A = 10$ km/s). The parameter space exploration reveals that frequency shifts exceeding 10% occur for amplitudes above 3 km/s, conditions frequently encountered in spicular jets and magnetic bright point oscillations. This suggests that nonlinear wave dynamics may be an inherent feature of the most energetic events in the lower solar atmosphere.

VII.a.3 Solar Atmospheric Implications

The solar application results (Figure 3b) indicate that nonlinear frequency shifts are most pronounced in regions with lower Alfvén speeds, typically found in denser chromospheric layers. This suggests that wave propagation through density inhomogeneities may experience spatially varying nonlinear

corrections, potentially leading to phase mixing and enhanced dissipation. For example, a wave packet propagating upward through the chromosphere encounters decreasing density and increasing Alfvén speed, which would reduce the local nonlinear frequency shift. This gradient could cause the wave to continuously adjust its dispersion characteristics, possibly leading to the formation of shocks or enhanced energy deposition.

VII.a.4 Wave Localization

The wave envelope structure in Figure 4(d) shows amplitude modulation consistent with modulational instability. This localization mechanism may explain observed intermittency in torsional wave signatures and contribute to the formation of discrete energy deposition sites in the chromosphere. The characteristic spatial scale of 10-20 km matches the width of individual spicules, suggesting a possible link between nonlinear wave dynamics and the structuring of chromospheric jets.

VII.b Comparison with Previous Work

Our results extend previous studies in several ways. First, [7] derived nonlinear equations for Alfvén waves but focused on homogeneous plasmas without providing comprehensive graphical analyses or explicit expressions for frequency shifts in solar parameters. Second, [8] studied nonlinear surface Alfvén waves but considered different geometry (slab versus cylindrical) and did not quantify the amplitude-dependent frequency shifts for torsional modes. Thirdly, [12] examined pulse propagation but did not derive complete dispersion relations or explore the parameter space as systematically as we have done here. Our graphical analyses provide quantitative predictions for frequency shifts and phase speed modifications that can be directly compared with observations from modern solar telescopes.

VII.c Observational Implications

The predicted frequency shifts ($\Delta\omega/\omega \sim 1 - 25\%$ for realistic amplitudes) have several observational implications for solar physics.

VII.c.1 Spectroscopic Signatures

High-resolution spectrometers may detect nonlinear frequency shifts through various spectroscopic signatures. Line broadening effects arise because enhanced frequencies correspond to larger Doppler shifts, potentially contributing to non-thermal line widths, and the quadratic amplitude dependence means that larger amplitude waves produce disproportionately broader lines. Phase speed variations can be detected through time-distance analysis of wave fronts, with the predicted phase speed enhancement of 0.4-2.5% being potentially measurable over long propagation paths. Additionally, the presence of second harmonic generation, implied by the nonlinear theory, may produce observable spectral features at twice the fundamental frequency, and detecting such harmonics would provide direct evidence of nonlinear wave-wave interactions in the solar atmosphere.

VII.c.2 Instrumental Requirements

Different solar observatories have varying capabilities for detecting these nonlinear effects. The Hinode/EIS instrument, with a velocity sensitivity of approximately 0.1 $\mathrm{km\,s^{-1}}$, could detect relative frequency shifts $\Delta\omega/\omega \sim 1\%$ for typical conditions, corresponding to wave amplitudes of about 1.5 km/s. The Daniel K. Inouye Solar Telescope (DKIST), with its superior velocity precision of ~ 0.03 $\mathrm{km\,s^{-1}}$, could measure nonlinear effects for amplitudes as low as 0.5 km/s, making it ideal for probing the weakly nonlinear regime. The Solar Orbiter/SPICE instrument may detect frequency shifts in extreme ultraviolet lines through periodic intensity variations, though the shorter wavelengths and higher temperatures characteristic of these observations may complicate interpretation.

VII.c.3 Wave Heating Efficiency

The modified dispersion relations significantly affect resonance conditions for wave heating mechanisms in the solar atmosphere. Phase speed enhancements may shift resonant layers within the atmosphere, thereby altering where wave energy is deposited. Frequency shifts could change wave transmission coefficients through the transition region, affecting the amount of energy that ultimately reaches the corona. Furthermore, the onset of modulational instability may create localized heating sites through wave breaking or shock formation, providing a potential mechanism for intermittent heating observed in the chromosphere and corona.

VII.d Limitations and Future Work

Several limitations of our analysis warrant mention. First, the zero-beta approximation, while valid in strongly magnetic regions such as magnetic bright points, breaks down in the upper chromosphere where $\beta \sim 1$, and finite-beta effects may modify the nonlinear coupling coefficients and introduce additional wave modes. Second, we have neglected atmospheric stratification and flux tube expansion, both of which introduce additional length scales and could modify the dispersion relations, suggesting that a more realistic model would include density and magnetic field gradients. Third, our analysis omits dissipation mechanisms including resistivity, viscosity, and radiation losses, which may compete with nonlinear effects especially for high-frequency waves, and dissipation could damp the modulational instability or alter the frequency shifts. Fourth, we assumed a straight, axisymmetric tube with a rigid boundary, neglecting curvature, twist, and interaction with the external plasma, all of which could affect wave propagation and stability.

Future work should address these limitations through several complementary approaches. This includes the inclusion of finite-beta effects and stratification in the analytical framework, perhaps using WKB methods for slow variations. Numerical simulations are needed to verify the nonlinear dispersion relations in realistic geometries and to explore the nonlinear evolution beyond the weakly nonlinear regime. The coupling with other wave modes such as kink and sausage modes should be investigated to study multi-mode propagation and energy transfer. Direct comparison with DKIST and Solar Orbiter observations of torsional wave signatures should be undertaken, using the predicted frequency shifts as a diagnostic tool. Finally, the investigation of nonlinear effects on wave reflection and transmission at atmospheric interfaces could provide crucial insights into how these processes influence the energy budget of the chromosphere and corona.

VIII Conclusion

The linear and nonlinear dispersion relations for torsional Alfvén waves traveling in zero-beta magnetic flux tubes have been methodically determined. The non-dispersive character of torsional Alfvén waves in a homogeneous medium is confirmed by the identical phase and group velocities $v_p = v_g = v_A$ obtained from the linear dispersion relation $\omega = kv_A$. As demonstrated by our graphical studies, the nonlinear analysis extends this to $\omega = kv_A + (k/v_A)|a|^2$, exposing a positive amplitude-dependent frequency shift that results from the combined impacts of mean flow generation and second harmonic creation. A nonlinear Schrödinger equation with focused cubic nonlinearity governs the amplitude evolution, resulting in modulational instability for any nonzero amplitude with a growth rate proportional to the square of the amplitude. Figures 3a and 3b illustrate the resultant frequency shifts, which follow $\Delta\omega/\omega = |a|^2/v_A^2$ and reach 1-25% for observed wave amplitudes. These changes may be detected with existing or next-generation solar telescopes. As $v_p = v_A(1 + |a|^2/v_A^2)$, the phase velocity rises with enhancements of 0.4–2.5% under solar circumstances, while the group velocity stays constant up to leading order. Finally, nonlinear effects are most significant for high amplitudes and low Alfvén speeds, according to the parameter dependency, suggesting that they are most important in thick chromospheric layers and in energetic events like spicules and jets. Nonlinear frequency changes become large ($> 1\%$)

for wave amplitudes exceeding 1 km/s, as shown by the graphical analysis that offer quantitative forecasts for solar atmosphere conditions. The chromosphere's intermittent energy deposition may be caused by these alterations, which may also affect wave heating processes through altered resonance circumstances.

For the interpretation of observations of torsional Alfvén waves in solar magnetic structures, these findings offer a thorough theoretical framework. The anticipated nonlinear effects could help with wave localization, energy dissipation, and improved mass transport in chromospheric jets and spicules. There will be fantastic chances to verify these hypotheses and improve our knowledge of MHD wave dynamics in the solar environment with future high-resolution observations from instruments like DKIST and Solar Orbiter.

Acknowledgments

This work was supported by the research facility provided by the Institute of Natural Sciences and Applied Technology, Kolkata. We acknowledge helpful discussions with the Sheffield Solar Physics research group.

Data Availability

The analytical derivations presented in this paper are self-contained. The data tables used to generate the figures are included in the manuscript text.

References

[1] E. Priest. *Magnetohydrodynamics of the Sun*. Cambridge University Press, Cambridge, 2014.

[2] J. P. Goedbloed and S. Poedts. *Principles of Magnetohydrodynamics*. Cambridge University Press, Cambridge, 2004.

[3] D. B. Jess, M. Mathioudakis, R. Erdélyi, P. J. Crockett, F. P. Keenan, and D. J. Christian. Alfvén waves in the lower solar atmosphere. *Science*, 323(5921):1582–1585, 2009.

[4] M. Stangalini, R. Erdélyi, C. Boocock, D. Tsiklauri, C. J. Nelson, D. Del Moro, F. Berrilli, and M. Korsós. Torsional oscillations within a magnetic pore in the solar photosphere. *Nature Astronomy*, 5:691–696, 2021.

[5] K. Shibata and Y. Uchida. Switching-on of winds and jets by magnetic twist. *Solar Physics*, 103(2):299–313, 1986.

[6] B. De Pontieu, S. W. McIntosh, M. Carlsson, V. H. Hansteen, T. D. Tarbell, C. J. Schrijver, A. M. Title, R. A. Shine, S. Tsuneta, Y. Katsukawa, K. Ichimoto, Y. Suematsu, T. Shimizu, and S. Nagata. Chromospheric alfvénic waves strong enough to power the solar wind. *Science*, 318(5856):1574–1577, 2007.

[7] J. V. Hollweg. Nonlinear alfvén waves and the solar wind. *Journal of Geophysical Research*, 76(31):7491–7502, 1971.

[8] M. S. Ruderman. Nonlinear surface alfvén waves. *Journal of Plasma Physics*, 63(5):443–461, 2000.

[9] R. J. Defouw. Wave propagation in magnetic flux tubes. *The Astrophysical Journal*, 209:266–269, 1976.

[10] B. Roberts and A. R. Webb. Magnetohydrodynamic waves in magnetic flux tubes i: Linear waves. *Solar Physics*, 56(1):5–35, 1978.

[11] B. Roberts and A. R. Webb. Magnetohydrodynamic waves in magnetic flux tubes ii: Nonlinear waves. *Solar Physics*, 64(1):77–92, 1979.

[12] J. Scalisi, W. Oxley, M. S. Ruderman, and R. Erdélyi. Propagation of torsional alfvén pulses in zero-beta flux tubes. *The Astrophysical Journal*, 911(1):39, 2021.

[13] S Thakur, P.and Kaur and M Devgan. Differential configurational entropy in nonlinear self-similar optical rogue wave. *Natural Sciences and Applied Technology*, 2(2):44, 2025.

[14] S.N Khanam, R.and Barman and D Mahanta. Ion acoustic solitary wave formation in a warm, unmagnetized dusty plasma with electron inertia. *Natural Sciences and Applied Technology*, 2(1):RA–25–MS–101, 2025.

[15] S. Mukherjee, M Majumdar, K Ghosh, J Kundu, and S.K Sarkar. A theoretical model for nonlinear plasma waves using a modified kdv-burgers framework. *Natural Sciences and Applied Technology*, 2(2):RA–25–PS–205, 2025.

[16] K. Cho, J. Chae, E.-K. Lim, H. Park, K.-S. Cho, S.-C. Bong, and H. Kwak. Properties of solar magnetic bright points inferred from automated identification. *The Astrophysical Journal*, 881(1):4, 2019.

Apendices

A Detailed Derivation of Nonlinear Terms

A.a Mean Flow Equation

Starting from the momentum equation at order ϵ^2:

$$\begin{aligned}\frac{\partial \vec{v}_2}{\partial t_0} =& -(\vec{v}_1\cdot\nabla)\vec{v}_1 \\ &+\frac{1}{\mu_0\rho_0}\left[(\overrightarrow{\nabla}\times\vec{B}_2)\times\vec{B}_0+(\overrightarrow{\nabla}\times\vec{B}_1)\times\vec{B}_1\right].\end{aligned}$$

Time averaging ($\langle\cdot\rangle = \frac{1}{2\pi}\int_0^{2\pi}\cdot d\phi$) eliminates the left-hand side:

$$0 = -\langle(\vec{v}_1\cdot\nabla)\vec{v}_1\rangle + \frac{1}{\mu_0\rho_0}\left[\langle(\overrightarrow{\nabla}\times\vec{B}_2)\times\vec{B}_0\rangle + \langle(\overrightarrow{\nabla}\times\vec{B}_1)\times\vec{B}_1\rangle\right].$$

Compute each term:

$$\begin{aligned}\langle(\vec{v}_1\cdot\nabla)\vec{v}_1\rangle &= \frac{1}{2\pi}\int_0^{2\pi}\left(v_{\theta1}\frac{1}{r}\frac{\partial}{\partial\theta}\right)v_{\theta1}\vec{\theta}\,d\phi \\ &= -\frac{1}{r}\langle v_{\theta1}^2\rangle\vec{r} = -\frac{2|A|^2}{r}\vec{r}.\end{aligned}$$

$$\begin{aligned}\langle(\overrightarrow{\nabla}\times\vec{B}_1)\times\vec{B}_1\rangle &= -\left\langle\frac{\partial B_{\theta1}}{\partial z}B_{\theta1}\right\rangle\vec{z} \\ &= -\frac{B_0^2}{v_A^2}\epsilon^2\frac{\partial|A|^2}{\partial Z}\vec{z}.\end{aligned}$$

The axial component gives Equation (24).

A.b Second Harmonic Calculation

The $\phi_2 = 2\phi$ component of the momentum equation:

$$-2i\omega\vec{v}_2^{(2)} = -\frac{A^2}{r}\vec{r} - \frac{B_0^2}{\mu_0\rho_0 v_A^2}ikA^2\vec{z} + \frac{1}{\mu_0\rho_0}(\overrightarrow{\nabla} \times \vec{B}_2^{(2)}) \times \vec{B}_0.$$

The induction equation at this order:

$$-2i\omega\vec{B}_2^{(2)} = \overrightarrow{\nabla} \times (\vec{v}_2^{(2)} \times \vec{B}_0) - \frac{2i\omega B_0^2}{v_A^2}A^2 e^{2i\phi}\vec{\theta}.$$

Assuming solutions proportional to $e^{2i\phi}$ and solving the coupled system yields Equation (28).

B Derivation of NLS Equation Coefficients

The NLS equation coefficients come from the solvability condition at order ϵ^3. Consider the linear operator:

$$\mathcal{L} = \begin{pmatrix} \frac{\partial}{\partial t_0} & -\frac{B_0}{\mu_0\rho_0}\frac{\partial}{\partial z_0} \\ -B_0\frac{\partial}{\partial z_0} & \frac{\partial}{\partial t_0} \end{pmatrix} \begin{pmatrix} v_\theta \\ B_\theta \end{pmatrix}.$$

The adjoint operator is:

$$\mathcal{L}^\dagger = \begin{pmatrix} -\frac{\partial}{\partial t_0} & B_0\frac{\partial}{\partial z_0} \\ \frac{B_0}{\mu_0\rho_0}\frac{\partial}{\partial z_0} & -\frac{\partial}{\partial t_0} \end{pmatrix}.$$

The solvability condition requires that the inhomogeneous terms at order ϵ^3 are orthogonal to the null space of $\mathcal{L}^\dagger$. This yields:

$$\int_0^{2\pi} \begin{pmatrix} v_1^\dagger & B_1^\dagger \end{pmatrix} \begin{pmatrix} F_v \\ F_B \end{pmatrix} d\phi = 0,$$

where $(v_1^\dagger, B_1^\dagger) = (v_A/B_0, 1)e^{-i\phi}$ is the adjoint null vector, and (F_v, F_B) are the inhomogeneous terms. Evaluating this integral gives Equation (29) with coefficients:

$$P = \frac{v_A^2}{2\omega}, \quad Q = \frac{k}{v_A}.$$

Conflict of Interest: The Authors have no conflicts of interest to declare that they are relevant to the content of this article.